Shap. Mem. Superelasticity (2016) 2:371–379
DOI 10.1007/s40830-016-0084-x

SPECIAL ISSUE: ESOMAT 2015, INVITED PAPER

Magnetic Properties and Phase Diagram of $Ni_{50}Mn_{50-x}Ga_{x/2}In_{x/2}$ Magnetic Shape Memory Alloys

Xiao Xu[1] · Yasuki Yoshida[1] · Toshihiro Omori[1] · Takeshi Kanomata[1,2] · Ryosuke Kainuma[1]

Published online: 21 November 2016

Abstract $Ni_{50}Mn_{50-x}Ga_{x/2}In_{x/2}$ magnetic shape memory alloys were systematically prepared, and the magnetic properties as well as the phase diagram, including atomic ordering, martensitic and magnetic transitions, were investigated. The $B2$–$L2_1$ order–disorder transformation showed a parabolic-like curve against the Ga+In composition. The martensitic transformation temperature was found to decrease with increasing Ga+In composition and to slightly bend downwards below the Curie temperature of the parent phase. Spontaneous magnetization was investigated for both parent and martensite alloys. The magnetism of martensite phase was found to show glassy magnetic behaviors by thermomagnetization and AC susceptibility measurements.

Keywords Ferromagnetic shape memory alloys · Martensitic transformation · Ni-Mn-Ga-In · Phase diagram · Spontaneous magnetization

Introduction

The martensitic transformation behavior in the stoichiometric Ni_2MnGa Heusler alloy was first reported by Webster et al. in 1984 [1]. The report of magnetostrain due to rearrangement of martensite variants by the application of a magnetic field [2] greatly accelerated research on Ni–Mn–Ga alloys, and a large strain of over 10% has been reported [3, 4]. This family of alloys is called ferromagnetic shape memory alloys. On the other hand, represented by the Ni–Mn–In alloy [5, 6], metamagnetic shape memory alloys also show a considerably large magnetostrain with a sufficiently large output stress, which is realized by the magnetic field-induced reverse martensitic transformation.

For the Ni–Mn–Ga system, several magnetic phase diagrams based on the consideration of the average number of valence electrons per atom (e/a) [7] or a fixed Ga composition [8] have been reported. Recently, magnetic phase diagrams of the $Ni_{50}Mn_{50-x}Ga_x$ section have been reported [9, 10]. It has been found that the martensitic transformation starting temperature T_{M_s} in $Ni_{50}Mn_{50-x}Ga_x$ decreases with increasing Ga composition and that the T_{M_s} bends upwards when it is below the magnetic transition temperatures of parent (T_{C_P}) and martensite (T_{C_M}) phases [9]. However, in $Ni_{50}Mn_{50-x}In_x$, the opposite behavior has been found, i.e., the T_{M_s} bends downwards when it is below T_{C_P} [5]. Therefore, it is of fundamental interest to investigate a system of Ni–Mn–(Ga,In) to examine the Ga+In composition dependence of T_{M_s} when it intersects with the magnetic transition temperatures. While several researches have been done focusing on different sections, such as $Ni_{50}Mn_{25}Ga_{25-x}In_x$ by Khan et al. [11], $Ni_{50}Mn_{33}Ga_{17-x}In_x$ by Pramanick et al. [12], $Ni_{50}Mn_{34.5}Ga_{15.5-x}In_x$ by Takeuchi et al. [13] and $Ni_{57}Mn_{18}Ga_{25-x}In_x$ by Zhang et al. [14, 15], no systematic investigations have been performed based on the Ga:In = 1:1 equiatomic sections.

In this study, we chose a section of $Ni_{50}Mn_{50-x}Ga_{x/2}In_{x/2}$, which is just in the middle between the sections of $Ni_{50}Mn_{50-x}Ga_x$ and $Ni_{50}Mn_{50-x}In_x$. This is a follow up study to the talk we delivered at ESOMAT 2015 [16]. The

✉ Xiao Xu
xu@material.tohoku.ac.jp

[1] Department of Materials Science, Graduate School of Engineering, Tohoku University, Aoba-yama 6-6-02, Sendai 980-8579, Japan

[2] Research Institute for Engineering and Technology, Tohoku Gakuin University, Tagajo 985-8537, Japan

martensitic transformation temperatures, the $B2$–$L2_1$ order–disorder transformation temperature as well as the magnetic transition temperatures were determined. Moreover, the magnetic state of the martensite phase in $Ni_{50}Mn_{36}Ga_{14}$ and $Ni_{50}Mn_{34}Ga_{16}$ has been found to be ferromagnetic [9, 17], whereas that of $Ni_{50}Mn_{35}In_{15}$ has been reported to be blocking of magnetic clusters [18]. Therefore, the magnetic state of martensite phase was also studied in the $Ni_{50}Mn_{50-x}Ga_{x/2}In_{x/2}$ system with AC susceptibility measurements.

Experimental Procedures

$Ni_{50}Mn_{50-x}Ga_{x/2}In_{x/2}$ (GaInx) alloys with $x = 13$, 15, 16, 17, 18, 19, 20, 23, 25 and 30 were prepared by induction melting under an atmosphere of pure argon. The casted ingots were solution treated (ST) at 1173 K for 1 day followed by quenching in ice water. Ageing treatments at low temperatures followed. The ageing treatments were conducted at 673 K for 1 day if the $B2$–$L2_1$ order–disorder transition temperature T_t fulfilled $T_t \times 0.7 > 673$ K; otherwise, a two-step heat treatment of 873 K 1 day and 573 K 3 day was performed. Refer to "$B2$–$L2_1$ Order–Disorder Transition Temperature" section for the determination of T_t. The ageing conditions are listed in Table 1. Such ageing was done in an attempt to obtain a higher degree of atomic order, as had been performed in $Ni_{50}Mn_{50-x}Ga_x$ alloys [9]. All prepared samples were confirmed to show a single phase by microstructure observation (not shown) using a scanning electron microscope (SEM). The compositions were measured using an electron probe microanalyzer (EPMA) and the results are summarized in Table 1.

All measurements in this research were performed on aged samples unless otherwise indicated. Differential scanning calorimetry (DSC) under 10 K/min was applied for thermoanalysis. An argon flow atmosphere was used when the measurements were up to a temperature higher than 573 K; otherwise, an air atmosphere was used. A vibrating sample magnetometer (VSM) and a superconducting quantum interference device (SQUID) magnetometer were applied for thermomagnetization measurements in a helium atmosphere under 2 K/min. AC susceptibility measurements were conducted under an alternating magnetic field of 10 Oe by using the physical property measurement system (PPMS). Magnetization measurements were conducted at 6 K by the SQUID magnetometer.

Experimental Results

$B2$–$L2_1$ Order–Disorder Transition Temperature

Thermoanalysis was used to examine T_t in ST GaInx samples. As shown in Fig. 1a, T_t was clearly confirmed for these samples. Almost no hysteresis was found for the heating and cooling processes, which is the nature of the second-order transition. The determined T_t, which was defined as the peak temperature in the heating curve, is plotted against the composition in Fig. 1b. The dashed and dash-dot lines show the T_ts for $Ni_{50}Mn_{50-x}Ga_x$ [9, 19] and $Ni_{50}Mn_{50-x}In_x$ [20], respectively. The arrows show the corresponding vertex compositions. According to the Bragg–Williams–Gorsky (BWG) model, if the ordering of the $B2$ phase is perfect, the T_t is expected to follow a parabolic curve with the vertex appearing at a 25% composition [21, 22]. This is well fulfilled in $Ni_{50}Mn_{50-x}Ga_x$ [9, 19], but has an obvious deviation in $Ni_{50}Mn_{50-x}In_x$ [20]. The deviation in $Ni_{50}Mn_{50-x}In_x$ is not yet fully understood, but has been considered to be the effect of imperfect ordering in the $B2$ phase [20]. In $Ni_{50}Mn_{50-x}Ga_{x/2}In_{x/2}$, the vertex composition was found at

Table 1 Compositions, notations, solution-treatment (ST) and ageing treatment conditions for $Ni_{50}Mn_{50-x}Ga_{x/2}In_{x/2}$ alloys in this research

Norminal	Notation	Ni at.%	Mn at.%	Ga at.%	In at.%	ST	Ageing
$Ni_{50}Mn_{37}In_{6.5}Ga_{6.5}$	GaIn13	49.9 ± 0.2	37.3 ± 0.2	6.3 ± 0.1	6.5 ± 0.1	1173 K 1 day	873 K 1 day, 573 K 3 day
$Ni_{50}Mn_{35}In_{7.5}Ga_{7.5}$	GaIn15	50.3 ± 0.4	34.9 ± 0.3	7.2 ± 0.3	7.6 ± 0.2	1173 K 1 day	873 K 1 day, 573 K 3 day
$Ni_{50}Mn_{34}In_8Ga_8$	GaIn16	49.8 ± 0.1	34.1 ± 0.4	8.0 ± 0.2	8.1 ± 0.4	1173 K 1 day	673 K 1 day
$Ni_{50}Mn_{33}In_{8.5}Ga_{8.5}$	GaIn17	49.8 ± 0.8	33.4 ± 1.1	8.2 ± 0.2	8.6 ± 0.2	1173 K 1 day	673 K 1 day
$Ni_{50}Mn_{32}In_9Ga_9$	GaIn18	49.9 ± 0.2	32.2 ± 0.3	8.8 ± 0.2	9.1 ± 0.2	1173 K 1 day	673 K 1 day
$Ni_{50}Mn_{31}In_{9.5}Ga_{9.5}$	GaIn19	49.9 ± 1.1	31.3 ± 0.9	9.2 ± 0.2	9.6 ± 0.1	1173 K 1 day	673 K 1 day
$Ni_{50}Mn_{30}In_{10}Ga_{10}$	GaIn20	50.1 ± 0.4	30.0 ± 0.3	9.8 ± 0.2	10.1 ± 0.2	1173 K 1 day	673 K 1 day
$Ni_{50}Mn_{27}In_{11.5}Ga_{11.5}$	GaIn23	50.0 ± 0.3	27.2 ± 0.3	11.2 ± 0.3	11.6 ± 0.2	1173 K 1 day	673 K 1 day
$Ni_{50}Mn_{25}In_{12.5}Ga_{12.5}$	GaIn25	50.0 ± 0.2	25.2 ± 0.2	12.1 ± 0.2	12.7 ± 0.1	1173 K 1 day	673 K 1 day
$Ni_{50}Mn_{20}In_{15}Ga_{15}$	GaIn30	49.9 ± 0.2	20.2 ± 0.3	15.0 ± 0.3	14.9 ± 0.4	1173 K 1 day	673 K 1 day

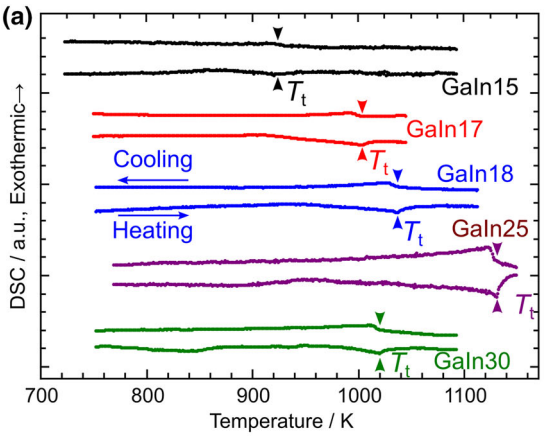

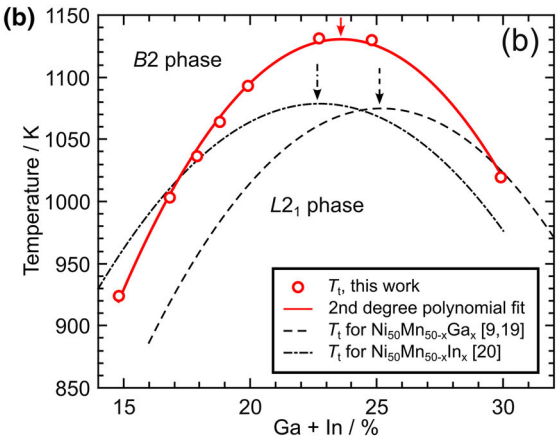

Fig. 1 **a** DSC curves at high temperatures for solution-treated (ST) $Ni_{50}Mn_{50-x}Ga_{x/2}In_{x/2}$ (GaInx) alloys. T_t shows the $B2$–$L2_1$ order–disorder transition temperatures. **b** T_t is plotted against the composition of Ga+In. *Solid line* shows the 2nd degree polynomial fit. Results reported for $Ni_{50}Mn_{50-x}Ga_x$ [9, 19] and $Ni_{50}Mn_{50-x}In_x$ [20] are plotted as *dashed* and *dash-dot lines*, respectively

around 23.6%, which lies between those of $Ni_{50}Mn_{50-x}Ga_x$ and $Ni_{50}Mn_{50-x}In_x$. However, the T_t at the vertex is much higher compared to those of $Ni_{50}Mn_{50-x}In_x$ and $Ni_{50}Mn_{50-x}Ga_x$. This is advantageous for obtaining a higher degree of atomic order for the $L2_1$ structure by ageing treatments, but the reason for this has not been revealed by the present study.

Ageing heat treatments were conducted according to the determined T_ts. Thus GaIn13 and GaIn15 alloys were subjected to two-stage ageing, as listed in Table 1.

Determination of Magnetic and Martensitic Phase Diagram

Martensitic transformation temperatures T_{M_s} and T_{A_f} and magnetic transition temperatures T_{C_P} and T_{C_M} were measured for the determination of the phase diagram.

Figure 2a shows the results of thermoanalysis for GaIn13, GaIn15 and GaIn16. Sharp peaks were detected for both the heating and cooling processes. T_{M_s} and T_{A_f} are defined by extrapolation as shown in the figure. The same samples were also subjected to thermomagnetization measurements. As shown in Fig. 2b, T_{M_s} was found to have a good consistency whereas DSC results showed higher T_{A_f}s than those from thermomagnetization. This was caused by the latency from the signal time constant of the DSC sensor. Both the results are listed in Table 2, whereas those by thermomagnetization should be used for the evaluation of the true transformation hysteresis.

Thermomagnetization measurements were also used to determine the magnetic transition temperatures. As shown in Fig. 3, T_{C_P} and T_{C_M} are detected for these samples, which are defined as the temperature at which the derivative of magnetization against temperature dM/dT shows a minimum value. In Fig. 3, the measurements were initiated by cooling

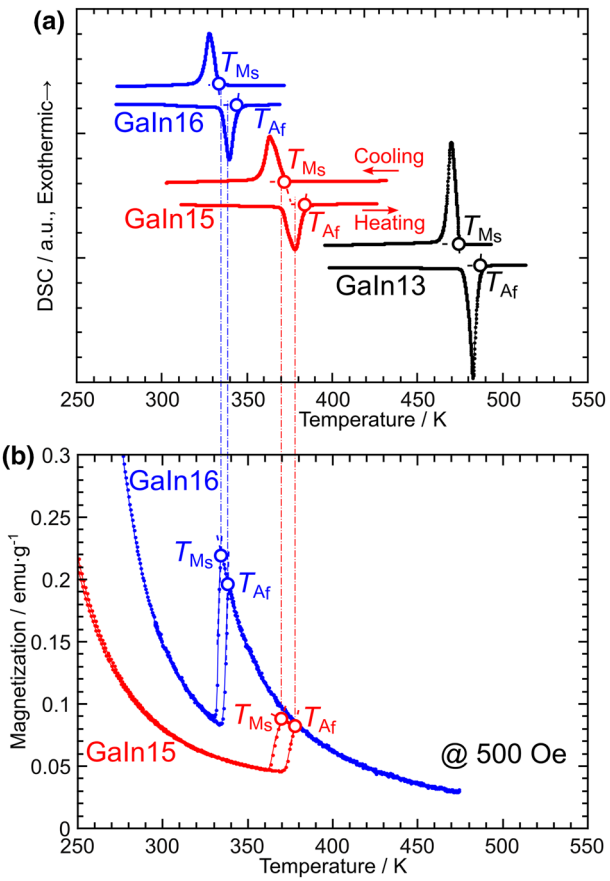

Fig. 2 **a** DSC and **b** thermomagnetization curves at low temperatures for $Ni_{50}Mn_{50-x}Ga_{x/2}In_{x/2}$ (GaInx) alloys. The martensitic transformation starting temperature T_{M_s} and the reverse martensitic transformation finishing temperature T_{A_f} were determined

from 380 K under a magnetic field of 500 Oe and followed by heating under the same magnetic field. Note the data shown here for GaIn15 are exactly the same as in Fig. 2b except for the scale of the vertical axis. Since the martensitic

Table 2 $B2$–$L2_1$ order–disorder transition temperature (T_t), martensitic transformation temperatures (T_{M_s} and T_{A_f}), magnetic transition temperatures for parent (T_{C_P}) and martensite (T_{C_M}) phases and spontaneous magnetization (M_{sp}) at 6 K for the $Ni_{50}Mn_{50-x}Ga_{x/2}In_{x/2}$ alloys in this research

Notation	Transformation Temperatures/K					Spontaneous Magnetizations, M_{sp}	
	T_t	T_{M_s}	T_{A_f}	T_{C_P}	T_{C_M}	emu g^{-1}	μ_B f.u.$^{-1}$
GaIn13		474†	487†	-	-	0	0
GaIn15	924	370	378	-	190	31.0	1.39
		372†	384†				
GaIn16		334	338	-	238	38.7	1.74
		333†	344†				
GaIn17	1004	278	285	306	-	48.2	2.18
GaIn18	1037	208	225	305	-	58.9	2.68
GaIn19	1065	107	147	320	-	70.0	3.20
GaIn20	1094	-	-	314	-	99.9	4.60
GaIn23	1132	-	-	325	-	89.2	4.18
GaIn25	1130	-	-	329	-	87.3	4.14
GaIn30	1020	-	-		-		

T_t was determined using thermoanalysis while T_{C_P} and T_{C_M} were determined using thermomagnetization measurements. For T_{M_s} and T_{A_f}, the results by thermoanalysis are shown following a dagger (†) while those by thermomagnetization measurements are shown as is. "-" indicates that the physical quantity does not exist and unmeasured values are left blank

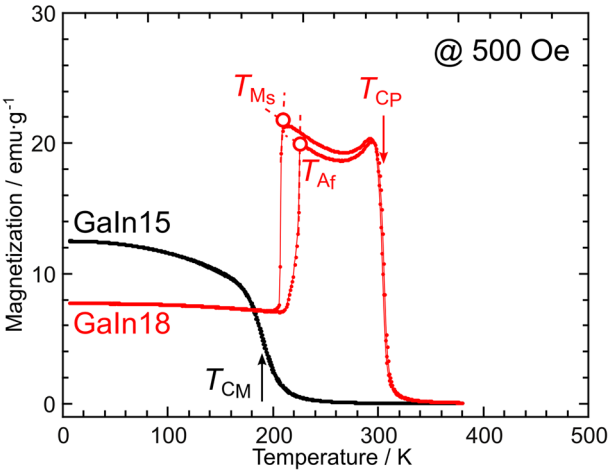

Fig. 3 Results of thermomagnetization measurements under 500 Oe for $Ni_{50}Mn_{50-x}Ga_{x/2}In_{x/2}$ (GaInx) alloys. T_{M_s} and T_{A_f} were determined for the martensitic transformation. Magnetic transition temperatures for the parent (T_{C_P}) and martensite (T_{C_M}) phases are also indicated

transformation occurs at about 370 K, the magnetic transition detected here is for the martensite phase.

T_{M_s}, T_{C_P} and T_{C_M} are summarized in Table 2 and plotted against the composition (Ga+In in at.%) in Fig. 4. It can be

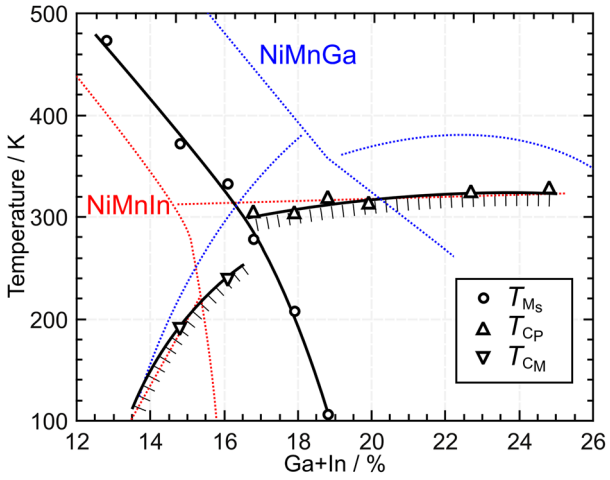

Fig. 4 T_{M_s}, T_{C_P} and T_{C_M} are plotted against composition (Ga+In in atomic percent) for the $Ni_{50}Mn_{50-x}Ga_{x/2}In_{x/2}$ (GaInx) alloys. *Solid lines* are guides for the eye. Results reported for $Ni_{50}Mn_{50-x}In_x$ [5, 26] and $Ni_{50}Mn_{50-x}Ga_x$ [9] are also shown by *dotted lines*

seen that while T_{C_P} shows very little composition dependence, T_{C_M} increases rapidly as the composition increases. A so-called paramagnetic gap [23] can be found near GaIn17, which is a common feature of the metamagnetic shape memory alloys [5, 24, 25]. The T_{M_s} monotonically decreases with increasing Ga+In composition and bends downwards below the magnetic transition temperatures. This will be discussed in detail in "Effect of Magnetic Transitions on Martensitic Transformation" section. Compared with the magnetic phase diagrams of $Ni_{50}Mn_{50-x}In_x$ [5, 26] and $Ni_{50}Mn_{50-x}Ga_x$ [9], which are also shown here as dotted lines, T_{C_M} and T_{C_P} were found to show almost the same tendency as in the case of $Ni_{50}Mn_{50-x}In_x$. For the T_{M_s}, though the gradient above magnetic transitions is almost the same as those for $Ni_{50}Mn_{50-x}In_x$ and $Ni_{50}Mn_{50-x}Ga_x$, it is closer to $Ni_{50}Mn_{50-x}In_x$ despite the fact that the alloys in this work have an almost perfect Ga:In = 1:1 composition ratio. The thermal transformation arrest (TTA) phenomenon [25, 27, 28] is not directly observed in GaInx alloys, and the arrest temperature T_A, if it exists, is expected to be lower than about 100 K.

Spontaneous Magnetization of $Ni_{50}Mn_{50-x}Ga_{x/2}In_{x/2}$ Alloys

Magnetization measurements were performed at 6 K for GaInx alloys to obtain spontaneous magnetization near the ground states. As shown in Fig. 5a, all the alloys except for GaIn13 clearly show spontaneous magnetization. At 6 K, GaIn13–19 alloys are in the martensite phase, whereas Ga20–25 alloys are in the parent phase. Their initial susceptibilities were also found to show large differences even in polycrystalline samples, which is related to the large

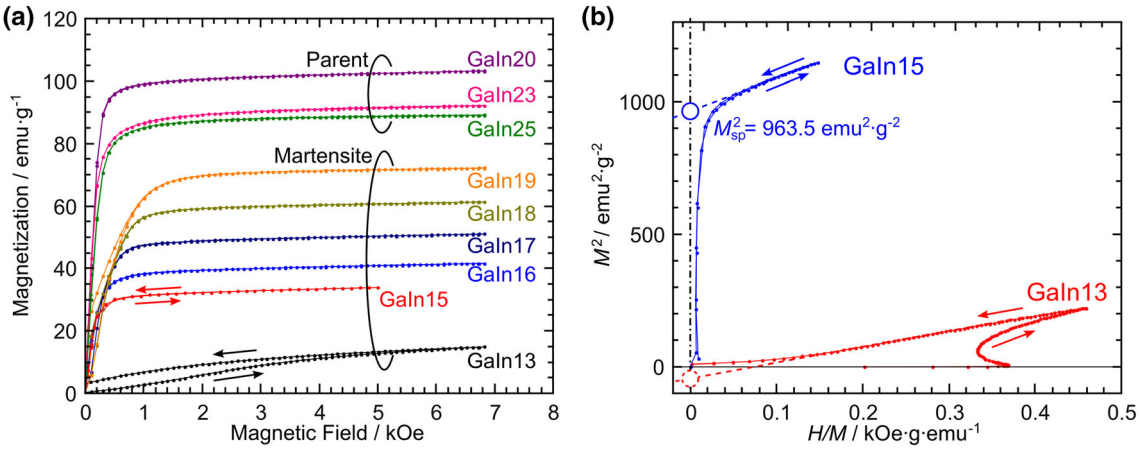

Fig. 5 **a** Magnetization curves at 6 K for $Ni_{50}Mn_{50-x}Ga_{x/2}In_{x/2}$ (GaIn*x*) alloys. **b** M^2 is plotted against H/M (Arrott plot [29]) for obtaining the spontaneous magnetization, M_{sp}. While the spontaneous magnetization was detected for GaIn15 and other alloys, the GaIn13 alloy was found to show no spontaneous magnetization

magnetocrystalline anisotropy of the martensite phase. For GaIn13, as indicated by the arrows, a small hysteresis was found. However, this was not found for other samples. This nonergodic behavior is related to the glassy magnetic state of the martensite, which will be discussed in detail in "Glassy Magnetic State of the Martensite Phase" section. In Fig. 5b, an M^2 versus H/M plot (Arrott plot [29]) for GaIn13 and Ga15 alloys is shown. For GaIn15, the spontaneous magnetization can be determined. However, GaIn13 was found to show no spontaneous magnetization. The determined spontaneous magnetization in the units of both emu g^{-1} and μ_B f.u.$^{-1}$ are listed in Table 2.

The spontaneous magnetization determined from Fig. 5 is plotted against the composition in Fig. 6. The trend for the data of the martensite phase is shown by a solid line, whereas that for parent phase is shown by a dashed line. Earlier reports for $Ni_{50}Mn_{50-x}Ga_x$ [9], $Ni_{50}Mn_{50-x}In_x$ [30–32] and $Ni_{50}Mn_{50-x}Sn_x$ [24, 33, 34] are also shown for reference. It can be seen that though the trend for the martensite phase of GaIn*x* alloys is very similar to those of $Ni_{50}Mn_{50-x}In_x$ and $Ni_{50}Mn_{50-x}Ga_x$, that of the parent phase shows a behavior different from that of $Ni_{50}Mn_{50-x}In_x$. This will be discussed in detail in "Effect of Magnetic Transitions on Martensitic Transformation" section.

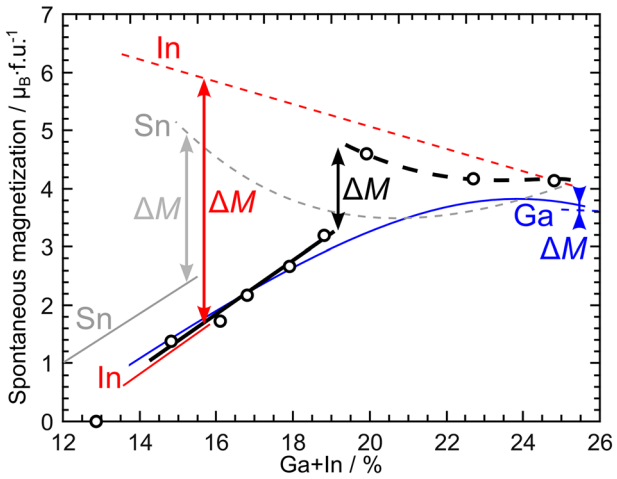

Fig. 6 Spontaneous magnetization at 6 K is plotted against the composition (Ga+In in atomic percent) for the $Ni_{50}Mn_{50-x}Ga_{x/2}In_{x/2}$ (GaIn*x*) alloys. The *solid* and *dashed lines*, which are guides for the eye, show the trends for martensite and parent phases, respectively. Results for $Ni_{50}Mn_{50-x}Ga_x$ [9], $Ni_{50}Mn_{50-x}In_x$ [30–32] and $Ni_{50}Mn_{50-x}Sn_x$ [33, 34, 38] are also shown in this figure. ΔM indicates the differences of the magnetization between the parent and martensite phases for these alloys

Discussion

Effect of Magnetic Transitions on Martensitic Transformation

In Fig. 4, the T_{M_s} was observed to bend downwards below T_{C_P}. Based on a qualitative consideration, this bending behavior is caused by the stability competition from the change of magnetic free energy; a higher magnetic transition temperature and a greater spontaneous magnetization result in stronger magnetic free energy [9, 24]. Since generally $T_{C_P} > T_{C_M}$ and $M_{sp_P} > M_{sp_M}$ are the case for $Ni_{50}Mn_{50-x}Ga_{x/2}In_{x/2}$ alloys, the magnetic free energy stabilizes the parent phase more than the martensite phase when T_{M_s} is below the magnetic transition temperatures, which is consistent with the result of the downward bending of T_{M_s}. This is also similar to the repulsive magneto-structural transition behavior for the $Ni_{50}Mn_{50-x}In_x$ alloys [26]. However, difference was also found by comparing the $Ni_{50}Mn_{50-x}Ga_{x/2}In_{x/2}$ and $Ni_{50}Mn_{50-x}In_x$

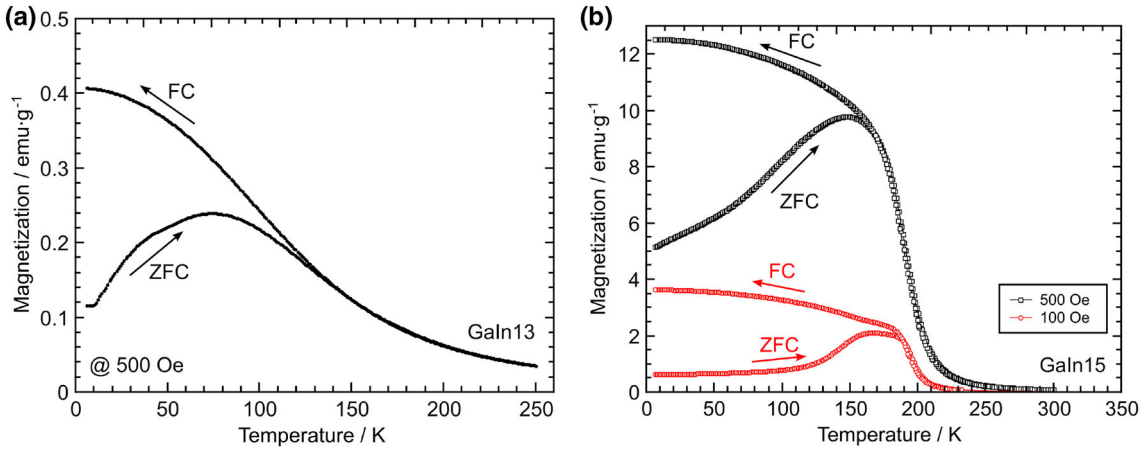

Fig. 7 Thermomagnetization measurements were conducted for **a** $Ni_{50}Mn_{37}Ga_{6.5}In_{6.5}$ (GaIn13) and **b** $Ni_{50}Mn_{35}Ga_{7.5}In_{7.5}$ (GaIn15) alloys. As indicated by the *arrows*, field-cooling (FC) measurements were conducted after the measurements of the zero-field-cooled (ZFC) samples

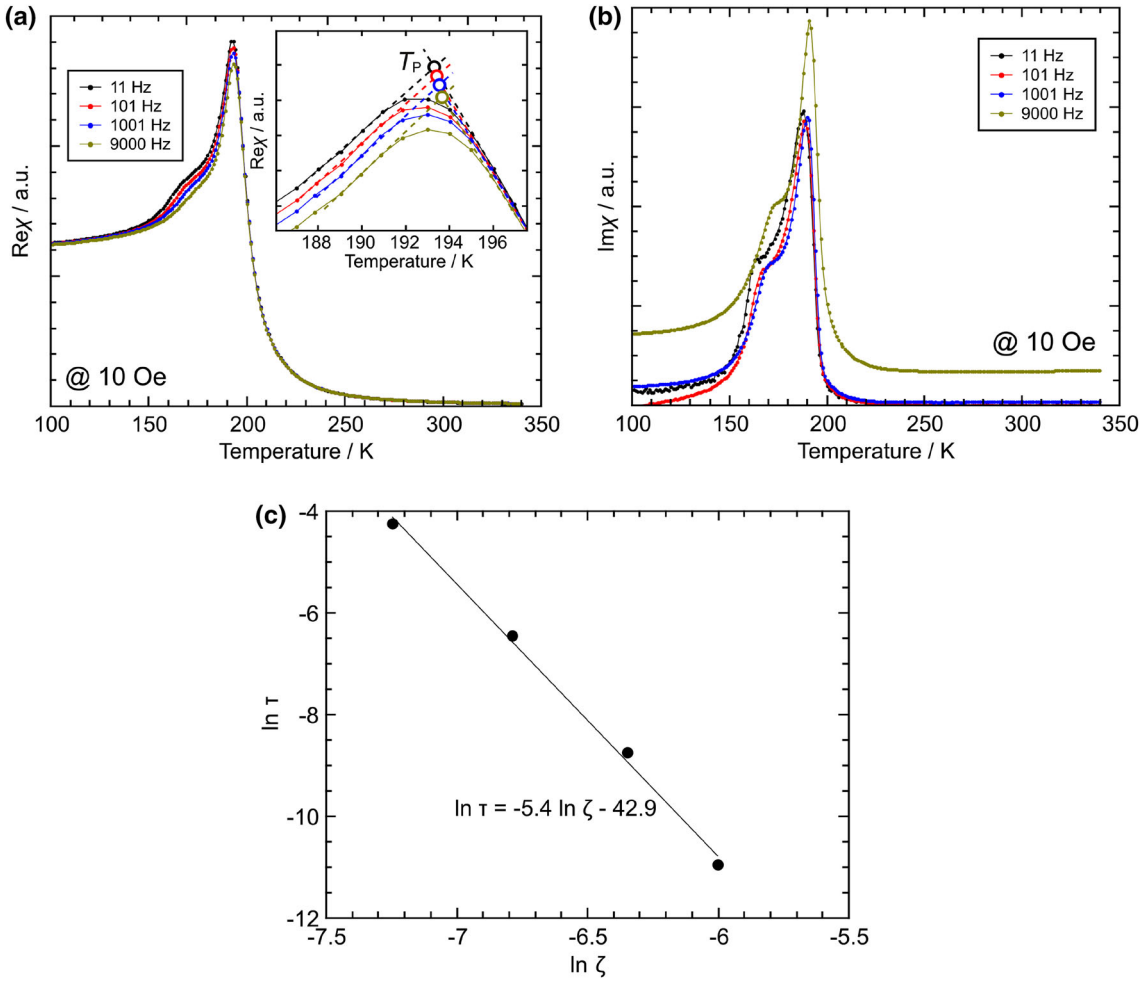

Fig. 8 Temperature dependence of linear magnetic susceptibility for $Ni_{50}Mn_{35}Ga_{7.5}In_{7.5}$ (GaIn15) alloy under an AC magnetic field of 10 Oe with frequencies of 11, 101, 1001 and 9000 Hz, with **a**) showing the real part and **b** showing the imaginary part. The temperature dependence of peak temperature T_P is substituted into Eq. 1 and $\ln \tau$ is plotted against $\ln \zeta$ in (**c**)

systems, i.e., the downward bending of T_{M_s} in $Ni_{50}Mn_{50-x}Ga_{x/2}In_{x/2}$ is less drastic than that in $Ni_{50}Mn_{50-x}In_x$. As shown in Fig. 4, since both the T_{C_M} and T_{C_P} of $Ni_{50}Mn_{50-x}Ga_{x/2}In_{x/2}$ alloys are very similar to those of $Ni_{50}Mn_{50-x}In_x$, the difference of magnetization (ΔM) is considered to be the main cause. First, as shown in Fig. 6, the ΔM in $Ni_{50}Mn_{50-x}Ga_{x/2}In_{x/2}$ is less than that in $Ni_{50}Mn_{50-x}In_x$ even though the Ga+In composition is the same as the In composition of $Ni_{50}Mn_{50-x}In_x$. Second, the position of T_{M_s} in $Ni_{50}Mn_{50-x}Ga_{x/2}In_{x/2}$ is to the right of $Ni_{50}Mn_{50-x}In_x$, as shown in Fig. 4. Since ΔM becomes smaller when the Ga+In composition is higher, as shown in Fig. 6, the ΔM in $Ni_{50}Mn_{50-x}Ga_{x/2}In_{x/2}$ becomes smaller than that in $Ni_{50}Mn_{50-x}In_x$ when the T_{M_s} is the same.

Moreover, as indicated by ΔM in Fig. 6, the alloys around GaIn19 show a jump in M_{sp}, where the parent phase is larger than that of martensite phase. Note that in $Ni_{50}Mn_{50-x}Ga_x$ alloys, the martensite phase generally has a larger M_{sp} than that of the parent phase [1, 9], whereas $Ni_{50}Mn_{50-x}In_x$ alloys show the opposite behavior [5, 30–32]. This suggests that the $Ni_{50}Mn_{50-x}Ga_{x/2}In_{x/2}$ alloys should also show metamagnetic behavior as in $Ni_{50}Mn_{50-x}In_x$ alloys.

Glassy Magnetic State of the Martensite Phase

As shown in Fig. 5a, a small hysteresis was found in the magnetization curve for the GaIn13 sample. This nonergodic behavior is further investigated in this subsection. Figure 7a, b show the thermomagnetization curves for GaIn13 and GaIn15 samples, respectively. For these measurements, the samples were zero-field-cooled (ZFC) to 6 K before measurements of the heating process under magnetic fields. The samples were then field-cooled (FC) back to 6 K under the same magnetic fields. Obvious splitting behaviors were found. In Fig. 7b, the magnetization measurement under a smaller magnetic field results in a stronger splitting behavior for the sample of GaIn15. The sample of GaIn15, which shows much stronger magnetization, was subjected to AC susceptibility measurements.

The measured real and imaginary parts of the linear susceptibilities are shown in Fig. 8a, b, respectively. As shown in the inset of Fig. 8a, which is a closeup of the temperature range near the magnetic transition, the peak temperature T_P shows obvious frequency dependence. Note that a similar behavior has been found for $Ni_{50}Mn_{50-x}In_x$ [18] whereas almost no frequency dependence has been found for $Ni_{50}Mn_{50-x}Ga_x$ [9]. In the spin-glass or similar systems, the standard theory of dynamical scaling near the phase transition is often used to analyze the frequency dependence. By following the power law [35, 36], the critical relaxation time τ is expressed as

$$\tau = 1/(2\pi f) = \tau^* \zeta^{-zv} \quad \text{with } \zeta = (T_P/T_f - 1), \tag{1}$$

where f is the frequency for the measurement, τ^* is the microscopic relaxation time (constant), ζ is the correlation length, zv is the dynamic critical exponent and T_f is the finite static freezing temperature, which is determined to be 193.2 K in this case. The plot of $\ln\tau$ against $\ln\zeta$ is shown in Fig. 8c. A linear relationship was found, and $zv = 5.4$, $\tau^* = 2 \times 10^{-19}$ were obtained. Note that the value of zv is very close to the value of 5.5 for $Ni_{35}Mn_{35}In_{15}$, $Ni_{35}Mn_{38.5}Sn_{11.5}$ and $Ni_{35}Mn_{40}Sb_{10}$ [18], and a value of zv in the range of 4–12 is typical for the case of a spin-glass system [35, 36]. However, the value of τ^* is very small compared to those between 10^{-12} and 10^{-14} reported for conventional metallic spin-glass systems [35, 36], suggesting a very weak interaction similar to the case of $La_{0.5}Ba_{0.5}CoO_3$ [37].

Conclusion

A systematic study of ordering, martensitic and magnetic transitions as well as magnetic properties was performed on the $Ni_{50}Mn_{50-x}Ga_{x/2}In_{x/2}$ magnetic shape memory alloys. The following conclusions were obtained according to the above experimental results.

- $B2$–$L2_1$ atomic order–disorder transformation temperatures were determined and were found to show a parabolic-like behavior with a vertex composition at around 23.6% Ga+In composition.
- A magnetic phase diagram including the martensitic transformation temperatures and magnetic transition temperatures was determined. The T_{M_s} monotonically decreases with increasing Ga+In composition, and slightly bends downwards below the magnetic transition temperatures.
- Composition dependence of spontaneous magnetization (M_{sp}) was investigated for both parent and martensite alloys. The M_{sp} was found to be higher in parent phase than that in the martensite phase, and the M_{sp} in parent phase was found to be lower than that in the $Ni_{50}Mn_{50-x}In_x$ system in M_{sp}-composition diagram.
- A glassy magnetic state was found in the martensite phase of $Ni_{50}Mn_{35}Ga_{7.5}In_{7.5}$ alloy by thermomagnetization and AC susceptibility measurements.

Acknowledgements This study was supported by a Grant-in-Aid for Scientific Research and by the Japan Society for the Promotion of Science (JSPS). A part of the low temperature experiments was performed at the Center for Low Temperature Science, Institute for

Materials Research, Tohoku University and Institute for Solid State Physics, the University of Tokyo.

References

1. Webster PJ, Ziebeck KRA, Town SL, Peak MS (1984) Magnetic order and phase-transformation in Ni_2MnGa. Philos Mag B 49(3):295–310
2. Ullakko K, Huang JK, Kantner C, O'Handley RC, Kokorin VV (1996) Large magnetic-field-induced strains in NiMnGa single crystals. Appl Phys Lett 69(13):1966–1968
3. Sozinov A, Likhachev AA, Lanska N, Ullakko K (2002) Giant magnetic-field-induced strain in NiMnGa seven-layered martensitic phase. Appl Phys Lett 80(10):1746–1748
4. Sozinov A, Lanska N, Soroka A, Zou W (2013) 12% magnetic field-induced strain in Ni–Mn–Ga-based non-modulated martensite. Appl Phys Lett 102(2):021902
5. Sutou Y, Imano Y, Koeda N, Omori T, Kainuma R, Ishida K, Oikawa K (2004) Magnetic and martensitic transformations of NiMnX(X = In, Sn, Sb) ferromagnetic shape memory alloys. Appl Phys Lett 85(19):4358–4360
6. Kainuma R, Imano Y, Ito W, Sutou Y, Morito H, Okamoto S, Kitakami O, Oikawa K, Fujita A, Kanomata T, Ishida K (2006) Magnetic-field-induced shape recovery by reverse phase transformation. Nature 439(23):957–960
7. Lanska N, Soderberg O, Sozinov A, Ge Y, Ullakko K, Lindroos VK (2004) Composition and temperature dependence of the crystal structure of Ni–Mn–Ga alloys. J Appl Phys 95(12):8074–8078
8. Khovaylo VV, Buchelnikov VD, Kainuma R, Koledov VV, Ohtsuka M, Shavrov VG, Takagi T, Taskaev SV, Vasiliev AN (2005) Phase transitions in $Ni_{2+x}Mn_{1-x}Ga$ with a high Ni excess. Phys Rev B 72(22):224408
9. Xu X, Nagasako M, Ito W, Umetsu RY, Kanomata T, Kainuma R (2013) Magnetic properties and phase diagram of $Ni_{50}Mn_{50-x}Ga_x$ ferromagnetic shape memory alloys. Acta Mater 61(18):6712–6723
10. Çakır A, Righi L, Albertini F, Acet M, Farle M, Aktürk S (2013) Extended investigation of intermartensitic transitions in Ni–Mn–Ga magnetic shape memory alloys: a detailed phase diagram determination. J Appl Phys 114(18):183912
11. Khan M, Dubenko I, Stadler S, Ali N (2004) Magnetic and structural phase transitions in Heusler type alloys $Ni_2MnGa_{1-x}In_x$. J Phys 16(29):5259–5266
12. Pramanick S, Chatterjee S, Venkateshwarlu D, Ganesan V, De SK, Giri S, Majumdar S (2013) Revival of martensitic instability in Ga doped Ni–Mn–In alloys. Intermetallics 42:56–61
13. Takeuchi AY, Guimarães CE, Passamani EC, Larica C (2012) Enhancement of magnetocaloric properties near room temperature in Ga-doped $Ni_{50}Mn_{34.5}In_{15.5}$ Heusler-type alloy. J Appl Phys 111(10):103902
14. Zhang LF, Wang JM, Hua H, Jiang CB, Xu HB (2014) Tailoring the magnetostructural transition and magnetocaloric properties around room temperature: in-doped Ni–Mn–Ga alloys. Appl Phys Lett 105(11):112402
15. Liu JH, Wang JM, Zhang LF, Wang X, Hua H, Jiang CB (2015) Effect of isoelectronic substitution on phase transition and magnetic properties of $Ni_{57}Mn_{18}Ga_{25-x}In_x$ ($0 \le x \le 8$) alloys with Ni excess. J Appl Phys 117(15):153904
16. Xu X, Kainuma R, Kihara T, Ito W, Tokunaga M, Kanomata T (2015) Thermodynamics and kinetics of martensitic transformation in Ni–Mn-based magnetic shape memory alloys. MATEC Web Conf 33:01004
17. Xu X, Kanomata T, Kainuma R (2014) Specific heat and entropy change during martensitic transformation in $Ni_{50}Mn_{50-x}Ga_x$ ferromagnetic shape memory alloys. Acta Mater 79:159–167
18. Umetsu RY, Fujita A, Ito W, Kanomata T, Kainuma R (2011) Determination of the magnetic ground state in the martensite phase of Ni–Mn–Z (Z = In, Sn and Sb) off-stoichiometric Heusler alloys by nonlinear AC susceptibility. J Phys 23(32):326001
19. Overholser R, Wuttig M, Neumann D (1999) Chemical ordering in Ni–Mn–Ga Heusler alloys. Scr Mater 40(10):1095–1102
20. Miyamoto T, Ito W, Umetsu RY, Kainuma R, Kanomata T, Ishida K (2010) Phase stability and magnetic properties of $Ni_{50}Mn_{50-x}In_x$ Heusler-type alloys. Scr Mater 62(3):151–154
21. Gorsky W (1928) X-Ray examination of transformations in the alloy Cu Au. Z Phys 50(1–2):64–81
22. Bragg WL, Williams EJ (1934) The effect of thermal agitation on atomic arrangement in alloys. Proc R Soc A 145(855):699–730
23. Fabbrici S, Albertini F, Paoluzi A, Bolzoni F, Cabassi R, Solzi M, Righi L, Calestani G (2009) Reverse magnetostructural transformation in Co-doped NiMnGa multifunctional alloys. Appl Phys Lett 95:022508
24. Ito W, Imano Y, Kainuma R, Sutou Y, Oikawa K, Ishida K (2007) Martensitic and magnetic transformation behaviors in Heusler-type NiMnln and NiCoMnln metamagnetic shape memory alloys. Metall Mater Trans A 38A(4):759–766
25. Xu X, Ito W, Tokunaga M, Kihara T, Oka K, Umetsu RY, Kanomata T, Kainuma R (2013) The thermal transformation arrest phenomenon in NiCoMnAl Heusler alloys. Metals 3(3):298–311
26. Kataoka M, Umetsu RY, Ito W, Kanomata T, Kainuma R (2013) Repulsive magneto–structural interaction in the ferromagnetic shape memory alloys $Ni_2Mn_{1+x}In_{1-x}$. J Magn Magn Mater 327:125–131
27. Sharma VK, Chattopadhyay MK, Roy SB (2007) Kinetic arrest of the first order austenite to martensite phase transition in $Ni_{50}Mn_{34}In_{16}$: DC magnetization studies. Phys Rev B 76(14):140401
28. Ito W, Ito K, Umetsu RY, Kainuma R, Koyama K, Watanabe K, Fujita A, Oikawa K, Ishida K, Kanomata T (2008) Kinetic arrest of martensitic transformation in the NiCoMnIn metamagnetic shape memory alloy. Appl Phys Lett 92(2):021908
29. Arrott A (1957) Criterion for ferromagnetism from observations of magnetic isotherms. Phys Rev 108(6):1394–1396
30. Krenke T, Acet M, Wassermann EF, Moya X, Mañosa L, Planes A (2006) Ferromagnetism in the austenitic and martensitic states of Ni–Mn–In alloys. Phys Rev B 73(17):174413
31. Kanomata T, Yasuda T, Sasaki S, Nishihara H, Kainuma R, Ito W, Oikawa K, Ishida K, Neumann KU, Ziebeck KRA (2009) Magnetic properties on shape memory alloys $Ni_2Mn_{1+x}In_{1-x}$. J Magn Magn Mater 321(7):773–776
32. Umetsu RY, Kusakari Y, Kanomata T, Suga K, Sawai Y, Kindo K, Oikawa K, Kainuma R, Ishida K (2009) Metamagnetic behaviour under high magnetic fields in $Ni_{50}Mn_{50-x}In_x$ (x=14.0 and 15.6) shape memory alloys. J Phys D 42(7):075003
33. Stager CV, Campbell CCM (1978) Anti-ferromagnetic order in Heusler alloy, $Ni_2Mn(Mn_xSn_{1-x})$. Can J Phys 56(6):674–677
34. Kanomata T, Fukushima K, Nishihara H, Kainuma R, Itoh W, Oikawa K, Ishida K, Neumann K, Ziebeck K (2008) Magnetic and crystallographic properties of shape memory alloys $Ni_2Mn_{1+x}Sn_{1-x}$. Mater Sci Forum 583:119–129
35. Binder K, Young AP (1986) Spin-glasses—experimental facts, theoretical concepts, and open questions. Rev Mod Phys 58(4):801–976

36. Mydosh J (1993) Spin glasses: an experimental introduction. Taylor and Francis, London
37. Kumar D, Banerjee A (2013) Coexistence of interacting ferromagnetic clusters and small antiferromagnetic clusters in $La_{0.5}Ba_{0.5}CoO_3$. J Phys 25(21):216005
38. Ito W, Xu X, Umetsu RY, Kanomata T, Ishida K, Kainuma R (2010) Concentration dependence of magnetic moment in $Ni_{50-x}Co_xMn_{50-y}Z_y$ (Z=In, Sn) heusler alloys. Appl Phys Lett 97(24):242512